Available online at www.sciencedirect.com

ScienceDirect

Geochimica et Cosmochimica Acta 297 (2021) 24–39

Geochimica et Cosmochimica Acta

www.elsevier.com/locate/gca

Restricted internal oxygen isotope exchange in calcite veins: Constraints from fluid inclusion and clumped isotope-derived temperatures

C.W. Nooitgedacht [a,*], H.J.L. van der Lubbe [a,b], S. de Graaf [c], M. Ziegler [d] P.T. Staudigel [b], J.J.G. Reijmer [a,e]

[a] Department of Geology and Geochemistry, Vrije Universiteit Amsterdam, De Boelelaan 1085, 1081 HV, Amsterdam, the Netherlands
[b] School of Earth and Ocean Sciences, Cardiff University, Park Place, Cardiff F10 3AT, United Kingdom
[c] Max Planck Institute for Chemistry, Hahn-Meitner-Weg 1, 55218 Mainz, Germany
[d] Earth Science Department, Utrecht University, Princetonlaan 8a, 3584 CB, Utrecht, the Netherlands
[e] College of Petroleum Engineering & Geosciences, King Fahd University of Petroleum & Minerals, Dhahran 31261, Saudi Arabia

Received 7 May 2020; accepted in revised form 11 December 2020; available online 5 January 2021

Abstract

The distribution of oxygen isotopes between calcite and fluid inclusions has demonstrated utility for reconstructing near-surface calcite precipitation temperatures. For calcite that formed at depth, however, the resilience of this paleothermometer to diagenetic oxygen isotope alteration is poorly constrained. Clumped isotopes also document calcite precipitation temperatures and are similarly vulnerable to diagenetic alteration. Post-entrapment isotope exchange between calcite and fluid-inclusions could alter the calcite-fluid oxygen isotope distribution ($\alpha_{c\text{-}fi}$), as well as the clumped isotope composition (Δ_{47}) of calcite, and therefore these two seemingly independent paleo-thermometers are potentially linked via the same alteration process. Using closed-system batch fractionation equations, we have modelled various scenarios of oxygen isotope exchange between water and host-rock during burial, as well as internal oxygen isotope exchange between calcite and fluid inclusions during exhumation. Assuming both paleo-thermometers record concordant temperatures at the time of vein formation, our models predict that if a fraction of calcite is available for isotopic interaction with fluid inclusions, the fluid inclusion and clumped isotope-derived paleothermometers yield discrepant temperature estimates after exhumation. We show that the fluid inclusion thermometer is more sensitive to isotopic alteration than the clumped isotope thermometer and that the mass balance of oxygen between calcite and fluid inclusions determines the sensitivity of both paleothermometers as well as the vulnerability of fluid inclusions ($\delta^{18}O_{fi}$) to diagenetic overprinting. We applied coupled clumped isotope and fluid inclusion measurements on calcite veins from the External Albanides (Albania), which were formed at depth and subsequently exhumed, in order to compare natural samples to our isotope exchange model. These veins show strongly discrepant calcite-water equilibrium temperatures and clumped isotope temperatures, suggesting the fraction of calcite available for isotope exchange with internal fluids may indeed be a key parameter of diagenetic alteration during exhumation. Even though the clumped isotope temperatures of our samples appear to be insensitive towards internal oxygen isotope exchange, our model predicts that at low burial temperatures, the carbonate clumped isotope thermometer may be susceptible to alteration by diagenetic isotope exchange with fluid inclusions under certain conditions.

Keywords: Fluid-inclusions; Clumped isotopes; Calcite veins; Oxygen isotope exchange; Paleo-thermometry

* Corresponding author.
E-mail address: c.w.nooitgedacht@vu.nl (C.W. Nooitgedacht).

https://doi.org/10.1016/j.gca.2020.12.008
0016-7037/

1. INTRODUCTION

The stable ($\delta^{18}O$ and $\delta^{13}C$) and clumped (Δ_{47} and Δ_{48}) isotopic compositions of carbonate minerals are widely used to study the composition, origin and temperature of paleofluids. Knowledge of the isotopic composition of paleofluids and crystallization temperature of minerals is of interest to researchers in a wide variety of earth-scientific domains. For instance, it has helped researchers deduce marine and terrestrial climatic conditions during specific geological time-intervals (Finnegan et al., 2011; Snell et al., 2013; Dennis et al., 2013; Price and Passey, 2013; Methner et al., 2016; Wierzbowski et al., 2018; Kelson et al., 2020), improve geodynamic models and constrain the diagenetic evolution of geological units (Huntington et al., 2011; Budd et al., 2013; Lacroix et al., 2014; Huntington and Lechler, 2015; Winkelstern and Lohmann, 2016; Mangenot et al., 2017; Macdonald et al., 2018; Staudigel et al., 2018; Honlet et al., 2018; Staudigel and Swart, 2019; Lacroix and Niemi, 2019; Naylor et al., 2019; Sundell et al., 2019; Elias et al., 2020; Beinlich et al., 2020), investigate the evolution and alteration of carbonatites (Fosu et al., 2020) and even deduce culinary techniques used by ancient cultures (Müller et al., 2017a,b; Staudigel et al., 2019).

When the calcite precipitation temperature is known, from for instance clumped isotope (Δ_{47}) paleothermometry, the relative abundance of ^{18}O in calcite, expressed as $\delta^{18}O_c$, can be used to calculate the $\delta^{18}O$ of the paleofluid ($\delta^{18}O_f$) from which the calcite precipitated (McCrea, 1950). Theoretically, precipitation temperatures can also be inferred from the distribution of oxygen isotopes between the $\delta^{18}O$ of calcite and the precipitating fluid. However, paleofluids are only rarely preserved due to the transient nature of fluids in geohydrological systems. With the advent of technological developments using on-line continuous flow spectrometry to measure fluid inclusion isotopes, it became possible to precisely determine the hydrogen and oxygen isotopic composition of fluid inclusions, expressed as $\delta^{2}H_{fi}$ and $\delta^{18}O_{fi}$, which may contain remnants of the precipitating fluid (Dennis et al., 2001; Vonhof et al., 2006; Dublyansky and Spötl, 2009; Arienzo et al., 2013; Affolter et al., 2014; Uemura et al., 2016). The fractionation factor between $\delta^{18}O_c$ and $\delta^{18}O_{fi}$, expressed as $\alpha_{c\text{-}fi}$, allows estimates of carbonate precipitation temperature, without relying on *a priori* assumptions regarding the $\delta^{18}O$-paleofluid variable, assuming precipitation in isotope equilibrium. The fractionation factor $\alpha_{c\text{-}fi}$, is defined as:

$$\alpha_{c-fi} = \frac{\delta^{18}O_c + 1000}{\delta^{18}O_{fi} + 1000} \quad (1)$$

in which subscripts 'c' and 'fi' denote the calcite and fluid-inclusion phases respectively. The fractionation factor alpha can be converted to temperature according to various temperature calibrations, as various carbonate species obey type-specific fractionation laws (McCrea, 1950; Epstein and Mayeda, 1953; Kim and O'Neil, 1997; Coplen, 2007; Tremaine et al., 2011; Daëron et al., 2016).

A major concern when interpreting the isotopic composition of fluid inclusions and using the fractionation factor $\alpha_{c\text{-}fi}$ for temperature reconstructions, is that the original composition of fluid inclusions might be affected by isotope exchange reactions that occur after fluid entrapment, as was for example experimentally demonstrated in speleothem fluid inclusions by Uemura et al. (2019). Exchange reactions are likely to affect fluid inclusions to a greater degree when they have faced high temperatures and pressures over long periods of time. For example, de Graaf et al. (2020) showed that uplift-related cooling of calcite veins from the Harz Mountains led to lowering of the $\alpha_{c\text{-}fi}$-derived paleotemperatures ($T\alpha_{c\text{-}fi}$) and depletion of $\delta^{18}O_{fi}$ values, caused by post-entrapment oxygen isotope equilibration. Comparably, unrealistically low $T\alpha_{c\text{-}fi}$ values were reported for calcite veins from the external Albanides (de Graaf et al., 2019), which are examined in this study.

The formation temperature of calcite veins can also be independently constrained using the clumped isotope thermometer (e.g. Budd et al., 2013; Bergman et al., 2013; Luetkemeyer et al., 2016; Sample et al., 2017; Burgener et al., 2018; Staudigel et al., 2018; Pagel et al., 2018), which relies upon the accurate measurement of the abundance of rare isotope bonds (for instance the ^{13}C-^{18}O bond) in the carbonate ion. The enrichment of these bonds compared to the stochastic distribution of isotope bonds (expressed as Δ_{47} or Δ_{48}), is related to the temperature at which the mineral formed ($T\Delta_{47}$; Ghosh et al., 2006). As the exchange of oxygen between calcite and fluid inclusions has the potential to alter the distribution of oxygen isotopes between the fluid and solid phase (thereby affecting $T\alpha_{c\text{-}fi}$), it will also break and reform C-O bonds within the calcite, simultaneously affecting $T\Delta_{47}$ (Stolper et al., 2018). Therefore, assessing coexisting $T\alpha_{c\text{-}fi}$ and $T\Delta_{47}$ provides a unique opportunity to constrain the parameters that possibly govern internal diagenetic alteration reactions in the calcite mineral. To study the effects of calcite diagenetic alteration reactions in a burial-exhumation setting, we have combined an isotope exchange model, in which the effect of diagenetic alteration on $T\alpha_{c\text{-}fi}$ and $T\Delta_{47}$ is calculated during exhumation, with measured $T\alpha_{c\text{-}fi}$ and $T\Delta_{47}$ data from calcite veins from the Ionian Zone of the External Albanides (southern Albania).

The External Albanides are home to a thick succession of homogeneous and fractured calciturbidites, wherein the vein system, its diagenetic properties and tectonic history have been well studied due to the presence of hydrocarbons in the region (Velaj et al., 1999; Nieuwland et al., 2001; Van Geet et al., 2002; Roure et al., 2004; Graham Wall et al., 2006; Vilasi et al., 2006; Le Goff et al., 2015; Le Goff et al., 2019). The calciturbidite succession is of Cretaceous to Paleocene age, and was buried to depths of 4 ± 1 km, at temperatures up to 100 °C (Van Geet et al., 2002; Roure et al., 2004; Vilasi, 2009; Lacombe et al., 2009). In this area, unrealistically low $\alpha_{c\text{-}fi}$ paleotemperatures were recorded by de Graaf et al. (2019), which might be the result of post-entrapment oxygen exchange.

To constrain the parameters that potentially govern isotope exchange reactions, fluid-calcite interaction was modelled using closed-system batch exchange reactions over a range of temperatures between maximum estimated burial temperatures and near surface temperatures. This approach

allows us to vary the size of the reservoirs involved in isotopic exchange and track the changes in $T\alpha_{c\text{-}fi}$ accordingly. The following stages of fluid modification are evaluated: (1) isotope exchange between water and host-rock during burial, (2) calcite vein formation and fluid entrapment, and (3) equilibration of fluid inclusions with vein calcite during uplift (Fig. 1). The final stage of fluid-carbonate exchange reactions affects both $T\alpha_{c\text{-}fi}$ and $T\Delta_{47}$, which is governed by the fraction of calcite that is available for isotope exchange with the fluid inclusions (the Calcite Exchange Fraction or CEF). This CEF parameter facilitates the decoupling between both paleothermometers during exhumation.

We determine the degree of isotopic alteration of fluid inclusions by comparing estimates of vein formation temperatures and fluid composition that are yielded by fluid inclusion and clumped isotope analysis. Our interpretation of the results assumes that, at the time of vein formation, these two paleothermometers gave concordant results and that present-day discordant results are related to oxygen equilibration processes that occurred after vein formation and fluid-entrapment. The analysis of $\delta^{18}O_c$, $\delta^{18}O_{fi}$ and Δ_{47} yields discrepant $T\alpha_{c\text{-}fi}$ and $T\Delta_{47}$ values, as is predicted by model scenarios in which part of the calcite available for isotopic exchange is highly restricted, suggesting that this parameter is of importance in post entrapment diagenetic calcite exchange. The model further predicts that, especially at a low CEF-value, the clumped isotope thermometer is less sensitive to isotopic alteration compared to the calcite-fluid thermometer, which is highly susceptible to diagenetic overprinting.

2. MATERIALS AND METHODS

2.1. Sample material

The veins that were used for this study were sampled from the Cretaceous to Paleocene calciturbidite interval in the Ionian Zone of the External Albanides. The calciturbidite interval is exposed in a series of folds and thrusts that dissect the basinal sediment succession of the former Ionian Basin, which consist predominantly of carbonates (Fig. 2). The carbonates are incorporated in a thin-skinned southwest-verging thrust system that was active from the late Oligocene to the lower Miocene, leading to the formation of three decoupled anticlinal belts: the Berati, Kurveleshi and Çika belt (Velaj et al., 1999; Meço et al., 2000). Their main décollement level is formed by Permo-Triassic evaporites, which provided flow pathways for fluids that circulated the Ionian basin deposits during their incorporation in the Albanide fold and thrust belt and led to the widespread formation of calcite veins (Vilasi, 2009).

We have analysed a total of 74 calcite veins, 4 calcite slickensides and 21 host rock samples from 21 outcrops across the Berati, Kurveleshi and Çika belts. In the field, veins were subdivided into populations according to their field orientation and vein morphology. The paragenetic sequence of vein formation was established by analysing the crosscutting relations between veins and stylolites, both in the field and petrographically. The vein populations were matched to the vein populations previously defined in studies performed by Graham Wall et al. (2006), Vilasi et al. (2006) and Vilasi (2009), and were categorized as V1, V2 or V3 veins, which link to different deformational phases that affected the Ionian Zone (de Graaf et al., 2019). We have selected clean (i.e. no mineralogical pollution) and undamaged (i.e. limited micro-cracks) calcite veins using optical microscopy (Nikon Eclipse 50i Polarizing Microscope) and cold cathodoluminescence microscopy (Olympus BX41). Fluid inclusions were examined petrographically using an Olympus FV3000 laser scanning confocal microscope (Fig. 3).

2.2. Analytical methods

2.2.1. Stable isotope analysis of carbonate

Carbon and oxygen isotope ratios of vein calcite and calciturbidite host-rock were analysed at the Earth Sciences

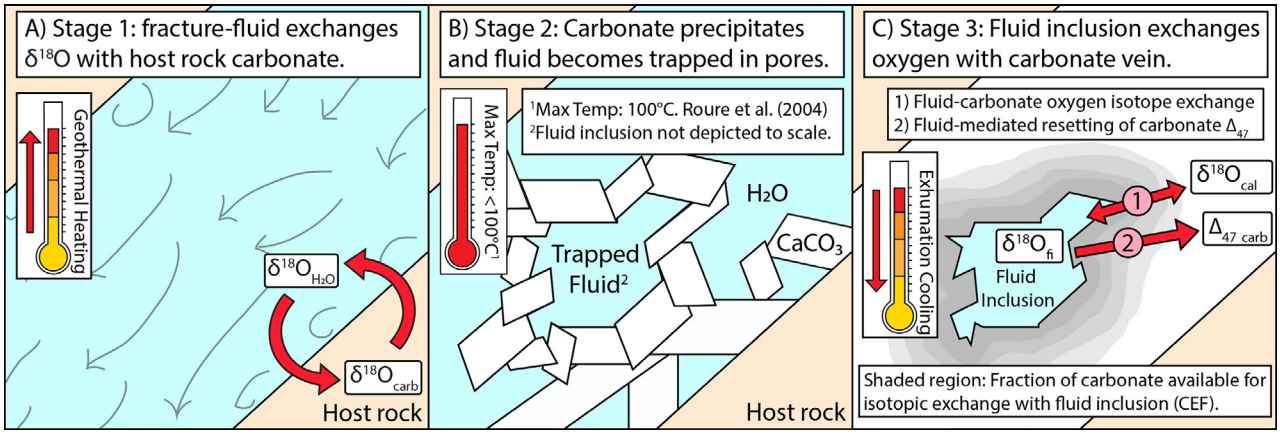

Fig. 1. Summary of the different stages of fluid modification by means of oxygen exchange before and after vein formation: (A) surface fluid infiltration and burial, and oxygen isotopes exchange with host rock. (B) Calcite precipitation and fluid entrapment at maximum burial temperatures of 100 °C. (C) Oxygen exchange between fluid inclusions and calcite within the fraction of calcite available for isotopic exchange, affecting the calcite and fluid phase, as well as the Δ_{47} values during cooling.

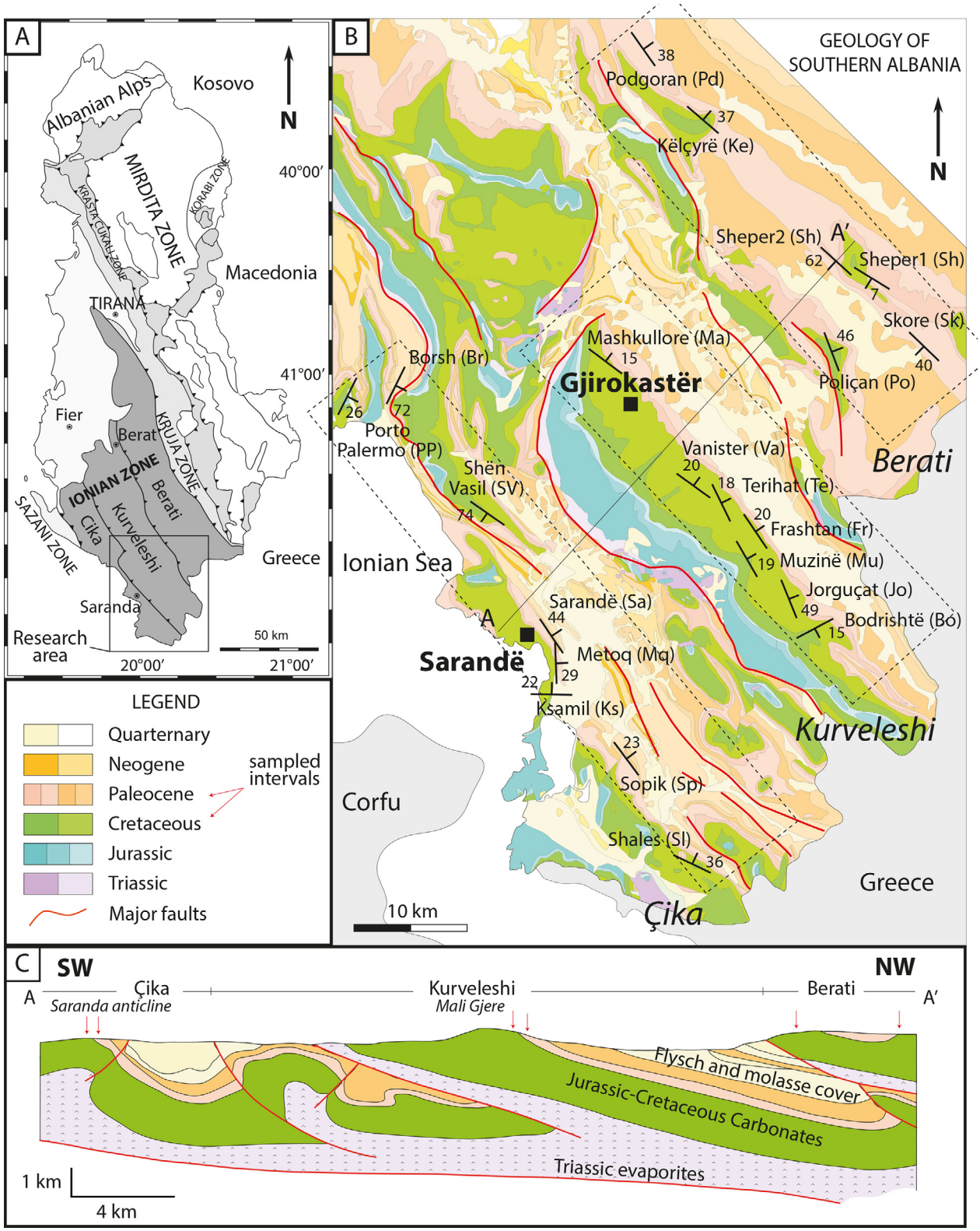

Fig. 2. (A) A map showing the main structural units of the research area indicated by the black square. (B) A geological map of southern Albania, 1:200000 (modified from de Graaf et al., 2019). Sampling stations are indicated with location name and bedding orientation, indicated by traditional strike-and-dip symbol with the short line pointing in the downward dip direction. Stippled squares group the sample locations according to structural belt. Red lines depict faults. (C) Schematic geological cross-section, A-A′ in the geological map, through the Ionian Zone (modified after Velaj, 2015; de Graaf et al., 2019). Red lines depict major décollements. (For interpretation of the references to colour in this figure legend, the reader is referred to the web version of this article.)

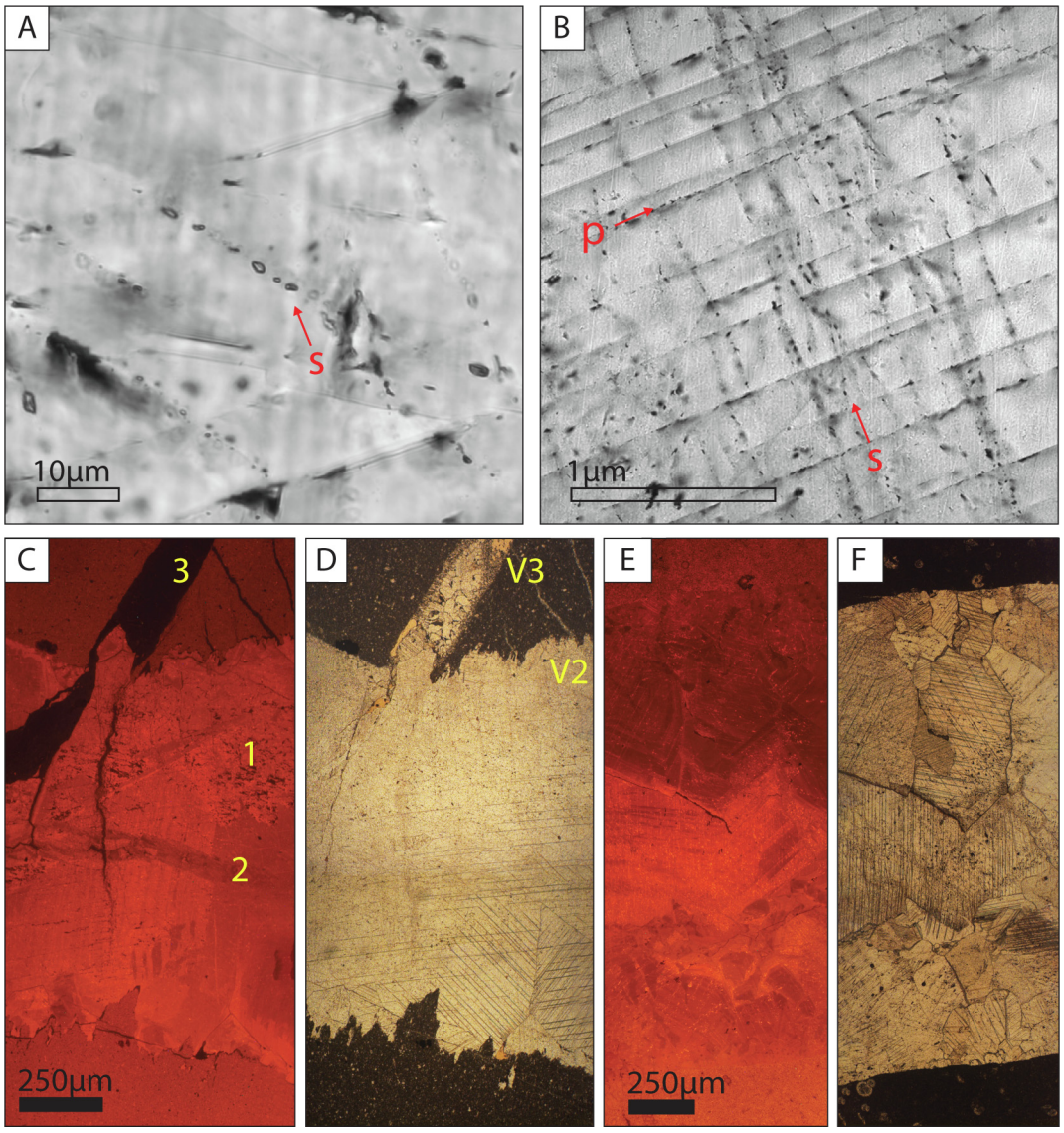

Fig. 3. (A, B) Confocal microscopy images showing irregular secondary (s) fluid inclusion trails. Primary fluid inclusions (p) align along crystal growth features. (C, D) Cathodoluminescence (CL) photographs and plane polarized light (PPL) equivalent. The image shows a dull orange luminescent V2 vein, which is dissected by a non-luminescent V3 vein. Recrystallization in this vein is associated with the stylolitization of the vein walls prior to the crosscutting by the V3 vein. The recrystallization is expressed by a contrast in brightness between the cathodoluminescent zones indicated by 1 and 2. The V3 vein that crosscuts this vein shows no luminescence. (E–F) CL and PPL equivalents show dull orange sector zonation within V1 calcite vein, which is typical for veins of the Ionian Zone.

Stable Isotope Laboratory at the Vrije Universiteit (VU) Amsterdam (The Netherlands), using a Thermo Finnigan Delta + mass spectrometer equipped with a GasBench II on-line gas preparation system operated at 45 °C. Routine analysis of a calcium carbonate standard, the IAEA-603, yielded average results of 2.46‰ for $\delta^{13}C$ and −2.42‰ for $\delta^{18}O$, and reproducibility was better than 0.1‰ for both $\delta^{13}C$ and $\delta^{18}O$. All $\delta^{13}C$ and $\delta^{18}O$ values of carbonate are reported against the VPDB scale.

2.2.2. Stable isotopes analysis of fluid inclusions

Hydrogen and oxygen isotope ratios of water from fluid inclusions in the calcite veins were measured at the Earth Sciences Stable Isotope Laboratory at the VU Amsterdam using a High-Temperature Conversion Elemental Analyzer (TC/EA), connected to a rock-crusher equipped with a cold-trap (Vonhof et al., 2006). This setup allows for on-line analysis of $\delta^{2}H$ and $\delta^{18}O$ values of fluid inclusion water from carbonate samples of up to 1.5 g. The crusher was operated at a constant temperature of 110 °C during the measurement procedure and samples were crushed 500 times to ensure maximum release of fluid-inclusion water. The cold-trap unit, used to focus the release of water to the TC/EA, was kept at −95 °C.

The minimum amount of water released per gram of vein calcite was estimated from measured intensity peaks of the crushed samples during isotope measurements proportionally to the intensity peaks from known volumes of

injected standard water before and after crushing. Routine analyses of an isotope standard, of which the composition approximates that of the fluid inclusions (DNS3: $\delta^2H = -9.5‰$, $\delta^{18}O = -1.43‰$ SMOW), indicate that the reproducibility of δ^2H was 1.4‰ and 0.1‰ for $\delta^{18}O$ over the course of fluid-inclusion measurements. The δ^2H_{fi} and $\delta^{18}O_{fi}$ values are reported against the SMOW-scale.

2.2.3. Clumped isotope analysis

The Δ_{47} compositions of selected calcite vein samples were analysed together with their $\delta^{13}C$ and $\delta^{18}O$ signatures at the stable isotope laboratory of the Utrecht University. The analyses were performed on 80–100 µg of sample by a Thermo Scientific MAT253-Plus connected to a KIEL IV device, wherein carbonate was digested in phosphoric acid at 70 °C (Meckler et al., 2014). From the acid digestion products, CO_2 was isolated by cryogenic traps. For sample gas purification, sample gas was transferred via a cooled (-40 °C) Porapak column (Meckler et al., 2014). Measurements are performed in long-integration dual inlet mode (LIDI) (Müller et al., 2017a,b). Pressure baselines were corrected based on daily peak shape scans (Meckler et al., 2014). The isotopic 'Brand' parameters were applied for calculation of Δ_{47} values (Brand et al., 2010; Daëron et al., 2016). Raw Δ_{47}values were transferred into the carbonate reference frame using carbonate standards ETH-1, ETH-2 and ETH-3 (Bernasconi et al., 2018), with a larger proportion of ETH-3 to minimize uncertainties in the final values (Kocken et al., 2019). The Δ_{47} values were converted to temperature according to the temperature calibration by Kele et al. (2015) and its recalculation by Bernasconi et al. (2018). Long-term standard deviation during the measurement period was around 0.03‰. The analysis of a single sample was repeated five to ten times to improve analytical precision. The maximum standard deviation of known replicates was 0.037‰.

2.3. Oxygen isotope exchange modelling

In order to understand to what extent fluid-mediated recrystallization could lead to anomalously low $T\alpha_{c\text{-}fi}$ values (de Graaf et al., 2019), a closed-system batch exchange model was developed. It simulates the exchange of oxygen isotopes between calcite and water, and its effect on the fractionation factor $\alpha_{c\text{-}fi}$ and Δ_{47} composition (Appendix 2). We separately modelled different stages of oxygen isotopic fluid modification in a typical burial-uplift setting (Fig. 1) and evaluated the effects of different parameters, such as host-rock composition, initial fluid composition, burial temperature and fluid-inclusion porosity for rock- and fluid-buffered systems.

The partitioning of oxygen isotopes between a fluid- and solid-phase was modelled using a closed-system oxygen isotope mass balance equation, in which the sum of the heavy isotopes in the product equals the sum of its precursors:

$$\delta^{18}O_A^1 M_A + \delta^{18}O_B^1 M_B = \delta^{18}O_A^2 M_A + \delta^{18}O_B^2 M_B \quad (2)$$

in which the constants, M_A and M_B correspond to the molar quantities of oxygen in the phases A and B, which are involved in the isotope exchange reaction and indices 1 and 2 indicate isotopic values before and after isotope exchange respectively. For our purposes, we assume that isotopic exchange between the two phases occurs at isotopic equilibrium, governed by a temperature-dependent fractionation factor (α) between the carbonate and mineral (Eq. (1)). Due to the kinetics at the calcite mineral growth surface, described in detail by Watkins and Hunt (2015), it is possible for the calcite to precipitate in a manner which deviates from expected equilibrium values. For this model, however, we assume "equilibrium" calcite formation relative to laboratory experiments at moderate growth rates (Kim and O'Neil, 1997):

$$1000\ln\alpha_{carb-H_2O} = 18.03\left(10^3 T^{-1}\right) - 32.42 \quad (3)$$

We also assume that molar quantities of oxygen in water and carbonate (i.e. M_f, M_s respectively) are the only relevant reservoirs of oxygen in the system, and therefore:

$$M_f + M_s = 1 \quad (4)$$

Eq. (1) can be then rewritten to:

$$\delta^{18}O_B^2 = (\delta^{18}O_A^2 + 1000)\alpha - 1000 \quad (5)$$

Successively, Eq. (2) can be rearranged to solve for the final fluid oxygen isotope composition:

$$\delta^{18}O_f^2 = \frac{\delta^{18}O_f^1(1 - M_s) + \delta^{18}O_s^1 M_s - 1000 M_s(\alpha - 1)}{M_f + \alpha M_s} \quad (6)$$

3. RESULTS

3.1. Stable isotopes of veins and host rock

The $\delta^{18}O$ values of calciturbidite host-rock occur in a narrow range between −2.9‰ and −1.0‰, typical of marine carbonates (Appendix 1). The average $\delta^{18}O$ composition of calcite veins is −3.7‰ with a range between −12.9‰ and 1.1‰. The lower $\delta^{18}O$ and broad range covered by the oxygen isotopes with respect to the host rock points to various degrees of water–rock interaction and/or multiple paleo-fluid sources.

The $\delta^{13}C$ isotopes of the calcite veins have values (−3.5‰ to 2.9‰) that cover a range comparable to that of the host-rock (0.21–2.42‰), suggesting that for the carbon isotope system, the fluids were buffered by the host-rock carbon reservoir prior to vein formation. Some anomalously low $\delta^{13}C$ values (i.e. −3.5‰) might be linked to methanogenic carbon isotope depletion (de Graaf et al., 2019). The paired $\delta^{13}C$ and $\delta^{18}O$ records of the calcite veins show no significant trend typical for late and near-surface diagenesis involving microbial decomposition of terrestrial organic matter and surface water infiltration (Knauth and Kennedy, 2009), suggesting that veins were unaffected by post-exhumation surface processes.

3.2. Stable isotopes of fluid inclusions

The $\delta^{18}O_{fi}$ values of fluid inclusions (subscript 'fi' denotes composition of fluid inclusions) range between −7.8 and 3.4‰ and δ^2H_{fi} values fall between −13 and

−48‰ (Fig. 4). The hydrogen and oxygen isotope data plot to the right of the modern global meteoric water line (GMWL) and form a continuum of values that range between GMWL values and more positive $\delta^{18}O$ values up to 4‰. These data show that, beside the temporal variation (i.e. between vein generations V1, V2 and V3) that was recorded by de Graaf et al. (2019) for the Kurveleshi belt, the average $\delta^{18}O$ composition also varies between the anticlinal belts (Fig. 4b and c). The reason behind these spatiotemporal variations is beyond the scope of this paper.

3.3. $T\alpha_{c\text{-}fi}$ and $T\Delta_{47}$

The oxygen isotope data of calcite and fluid inclusions allow for the estimation $T\alpha_{c\text{-}fi}$ based on the oxygen distribution between both phases (Fig. 5). $T\alpha_{c\text{-}fi}$ varies between −8° C to +57 °C, which is lower than most estimates of calcite formation temperatures based on primary fluid inclusion homogenisation temperatures (i.e. <80 °C; 95–120 °C; 34–60 °C and 45–145 °C; Vilasi, 2009). These homogenisation temperatures were recorded in veins from the Kelcyra outcrop in the Berati belt, but because these measurements were performed on individual inclusions while our analyses provide an integrate signal, the data were not adopted here. Comparable low $T\alpha_{c\text{-}fi}$ values have been previously reported for the Kurveleshi belt (de Graaf et al., 2019).

Four samples were selected for Δ_{47}-measurements (Fig. 4), based on the quality of the vein calcite and their associated deformational phase. Corrected Δ_{47} values fall between 0.555 and 0.514‰, which corresponds to $T\Delta_{47}$ estimates of 67 °C and 86 °C, respectively (Table 1; Bernasconi et al., 2018). The maximum standard error of the replicated unknowns was 0.014‰. Three samples yield similar average values of 84.5, 85.2 and 86.3 °C and one sample plots slightly lower, at 67.1 °C. Corresponding 95% confidence intervals range between 20.5 and 28.0 °C.

4. DISCUSSION

4.1. Discrepant paleotemperature results

The analysis of $\delta^{18}O_c$, $\delta^{18}O_{fi}$ and Δ_{47} in natural samples yields discrepant estimates of $T\alpha_{c\text{-}fi}$ and $T\Delta_{47}$. Assuming that both paleothermometers recorded concordant calcite precipitation temperatures during vein crystallization, we hypothesize that the offset between paleothermometers is the result of oxygen isotope exchange after fluid entrapment. This type of alteration, which is caused by temperature driven isotope exchange between calcite and water during recrystallization at the calcite-fluid inclusion interface, was recently experimentally demonstrated by Uemura et al. (2019) on speleothem calcite. Their results showed that the oxygen isotopes of fluid inclusions were able to exchange with 2 molar percent of the oxygen in the calcite when heated to 105 °C over a period of 80 hours.

Calcite veins that are being exhumed are exposed to cooling over a relatively long period of time, which is why calcite-fluid isotope exchange could affect a larger molar fraction of the carbonate-bound oxygen compared to the experimental speleothem calcite described above. In order to understand to what extent these alteration processes can actually affect clumped isotope and fluid inclusion $\delta^{18}O$ values, and what parameters control this, we have constructed an isotope exchange model that simulates burial conditions to which veins are typically exposed (i.e. vein formation temperatures, average host-rock composition and initial surface water composition). In this model, the co-evolution of $T\alpha_{c\text{-}fi}$ and $T\Delta_{47}$ is calculated for a

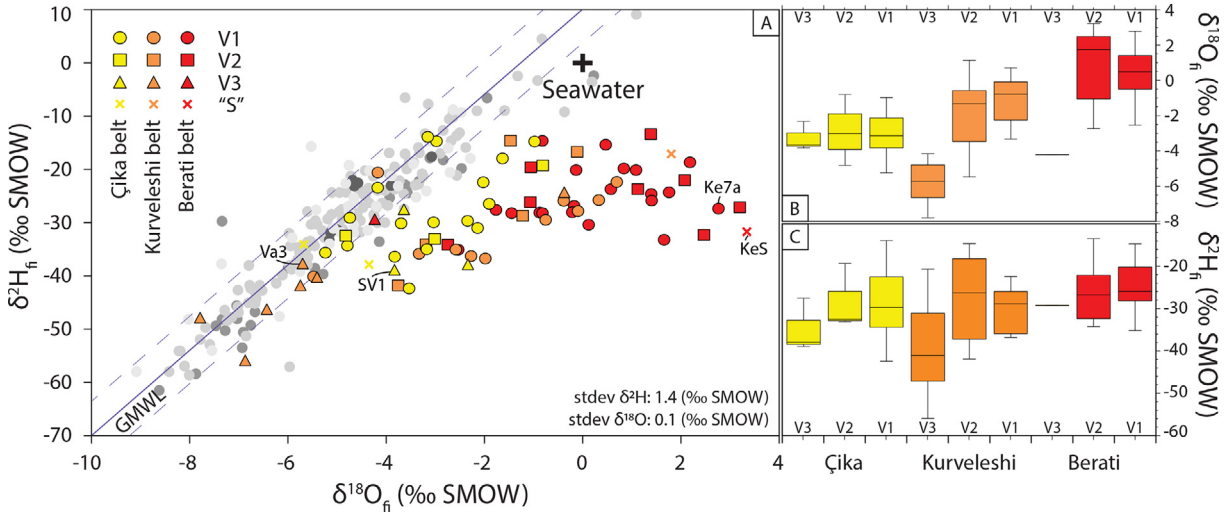

Fig. 4. (A) δ^2H_{fi} and $\delta^{18}O_{fi}$ data, categorized according to structural belts and vein populations (V1, V2, V3) and slickensides ("S"). Data from the Kurveleshi belt were taken from de Graaf et al. (2019). The grey circles indicate the modern meteoric water compositions at the nearby meteoric stations of Dubrovnik, Thessaloniki, Patras and Athens, measured between the year 2000 and 2005 (International Atomic Energy Agency, GNIP). The sample identification codes correspond to the samples that were analysed for clumped isotope thermometry. (B, C) Box and whisker plots for the $\delta^{18}O_{fi}$ and δ^2H_{fi} data grouped per anticlinal belt and vein population. (For interpretation of the references to colour in this figure legend, the reader is referred to the web version of this article.)

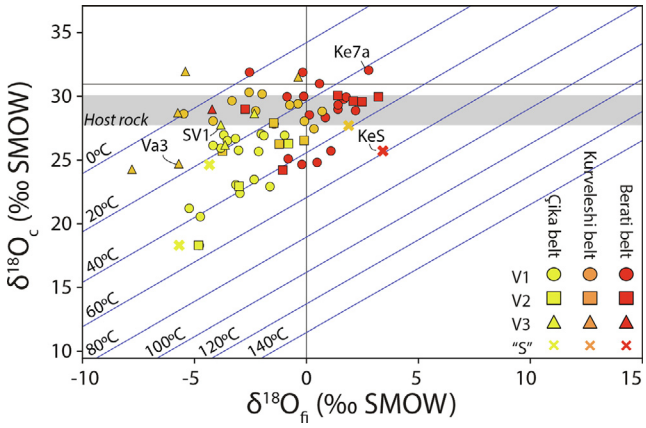

Fig. 5. $\delta^{18}O_c$ versus $\delta^{18}O_{fi}$ values of vein calcite and fluid inclusions. The blue lines indicate the isotherms based on Kim and O'Neil, (1997). The four samples that were selected for clumped isotope thermometry are indicated by their sample identification code. (For interpretation of the references to colour in this figure legend, the reader is referred to the web version of this article.)

system in which a vein forms at depth and is subsequently exhumed. The parameters that govern isotope exchange between the calcite vein and fluid inclusions can be evaluated by comparing the results of the modelled $T\alpha_{c\text{-}fi}$ and $T\Delta_{47}$ trajectories with measured $T\alpha_{c\text{-}fi}$ and $T\Delta_{47}$ data from the External Albanides.

4.2. Closed system oxygen isotope fractionation modelling

4.2.1. Stage 1: water–rock interaction during burial

In order to simulate stage 1 of fluid modification (i.e. closed-system interaction between water and host-rock carbonate; Fig. 1A), water–rock interaction prior to vein formation was modelled for different oxygen mass distribution scenarios. The calculation describing this stage predicts the alteration of the $\delta^{18}O_{fluid}$ and corresponding $\delta^{18}O_{host\text{-}rock}$ values at temperatures that range between maximum burial temperatures known for the various belts of the Ionian Zone (c. 100 °C) and near-surface temperatures (Fig. 6), whereby the $\delta^{18}O_{fluid}$ values increase and the $\delta^{18}O_{host\text{-}rock}$ values decrease with temperatures. The molar distribution of oxygen between water (f) and host rock (s) during these exchange reactions, which is here described as the fraction of oxygen in the fluid with respect to the total abundance of oxygen, $M_f/(M_s + M_f)$, has been modelled ranging from a water to a host-rock buffered system (note that this definition differs from the water–rock ratio, which is defined as M_f/M_s and ranges from 0 to ∞). Reconstructions of fluid-carbonate co-evolution in the Bahamas (Winkelstern and Lohmann, 2016; Staudigel and Swart, 2019) have determined that realistic values for the water–rock ratio in pore waters vary between 0.6–0.9 during burial up to 4 km, corresponding to a molar fraction of oxygen in fluid with respect to host rock between 0.38 and 0.47.

The behaviour of the $\delta^{18}O_{fluid}$ and $\delta^{18}O_{host\text{-}rock}$ values from surface towards burial temperatures depends not only on the water–rock mass distribution, but also on the initial fluid and host-rock composition and the effective calcite-water isotope equilibrium.

4.2.2. Stage 2: calcite precipitation and fluid entrapment

The second stage in our model involves the precipitation of calcite within a fracture. As calcite crystals grow, small amounts of fluid are trapped and form fluid inclusions. Once fluid inclusions are formed, the extent of isotopic exchange by microscopic dissolution-reprecipitation reactions between the fluid inclusions and calcite becomes restricted to the immediate surrounding of the fluid inclusion. This restriction is defined as the molar fraction of calcite available for exchange or Calcite Exchange Fraction (hereafter referred to as CEF). If, hypothetically, all calcite is available for isotopic exchange with fluid inclusions, then CEF equals 1. The CEF value approaches zero when the molar fraction of oxygen in calcite is restricted to calcite in the immediate surrounding of fluid inclusions. The CEF plays an important role in the decoupling of the results yielded by both paleothermometers during uplift in stage 3. The paleotemperatures that are recorded by both thermometers at the time that a calcite vein sample is fully exhumed are not affected by additional burial before or after vein formation, but depend only on the vein crystallization temperature, the compositional input and the relative size of the reservoirs between which oxygen isotopes exchange.

4.2.3. Stage 3: decoupling of the paleothermometers during exhumation

The final stage (3) of fluid modification involves the exchange of oxygen isotopes after vein formation, which occurs between the fluid inclusion and vein calcite by microscopic dissolution-reprecipitation (or recrystallization) reactions. This model relies on the simplification that these reactions occur continuously during exhumation. The exchange of oxygen between calcite and fluid is not necessarily uniformly distributed across the calcite vein mineralogy, as fluid inclusions may only be able to exchange with a limited portion of total calcite (Fig. 1c), as was observed in the heated speleothem fluid-inclusions by Uemura et al. (2019). In order to describe this restriction, the CEF was introduced, which limits the molar fraction of calcite that

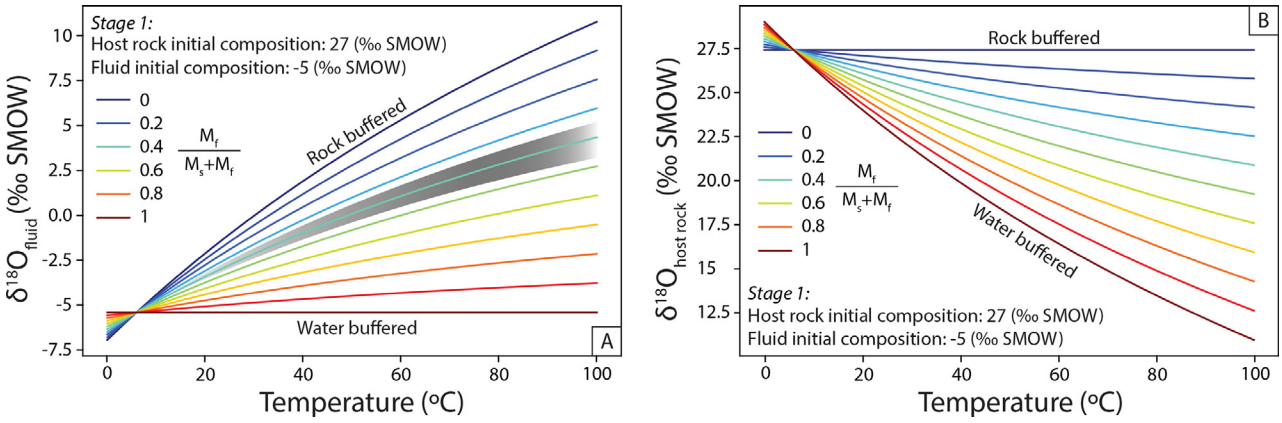

Fig. 6. Stage 1: $\delta^{18}O$ of fluids (A) and host rock (B) versus temperature for different water–rock interaction scenarios, here expressed as the fraction of oxygen in water with respect to the total volume of oxygen. Low water-to-rock ratios induce maximum depletion of $\delta^{18}O$ in fluids per degree Celsius and little enrichment for the corresponding host rock The shaded area corresponds to the water rock molar oxygen ratios reported by Winkelstern and Lohmann (2016) and Staudigel and Swart (2019), recalculated to satisfy the $M_f/(M_f + M_s)$ definition of water rock interaction. The maximum burial temperature was set to 100 °C, similar to the estimations of the maximum burial temperature of the calciturbidite reservoir in which the veins that are subject of this study are hosted (Van Geet et al., 2002; Roure et al., 2004).

exchanges isotopes with the fluid inclusions during uplift as follows:

$$M_{cal} = (1 - M_{fi})CEF \tag{7}$$

in which M_{cal} is the molar fraction of oxygen in calcite participating in isotopic exchange and M_{fi} represents the molar fraction of oxygen present in the fluid inclusions. Based on the amount of water released during the fluid-inclusion isotope analyses (Appendix 1) and a 10 percent estimate of crushing efficiency, the molar fraction of oxygen present in fluid inclusions per molar unit of calcite (M_{fi}) was estimated at 0.02. This estimation allows for the calculation of $\delta^{18}O$ compositions for fluid inclusions and calcite at various CEF scenarios during exhumation of a calcite vein (Fig. 7). Because the vast majority of oxygen exists in calcite compared to oxygen in fluid inclusions, the $\delta^{18}O_{fi}$ reacts more strongly to changes in temperature than the associated $\delta^{18}O_c$ composition.

During exhumation, the dissolution-reprecipitation reactions that facilitate the redistribution of oxygen isotopes between the fluid inclusions and host calcite within the limits of CEF, also facilitate the resetting of the clumped-isotope thermometer: as recrystallization occurs, the newly formed calcite records Δ_{47} temperatures correspond to the recrystallization temperature. In this way, the Δ_{47} and the $\alpha_{c\text{-}fi}$ values are linked and respond to temperature driven exchange following:

$$T\Delta_{47} = T_p(1 - CEF) + T_m CEF \tag{8}$$

and,

$$\alpha_{c-fi} = \frac{\delta^{18}O_{c(p)}(1 - CEF) + \delta^{18}O_{c(m)}CEF + 1000}{\delta^{18}O_{fi(m)} + 1000} \tag{9}$$

In which subscripts m and p refer to values at model (or cooling) temperature and precipitation temperature values, respectively. From the oxygen isotope distribution between calcite and fluid, $\alpha_{c\text{-}fi}$, corresponding temperatures were calculated using Eq. (3).

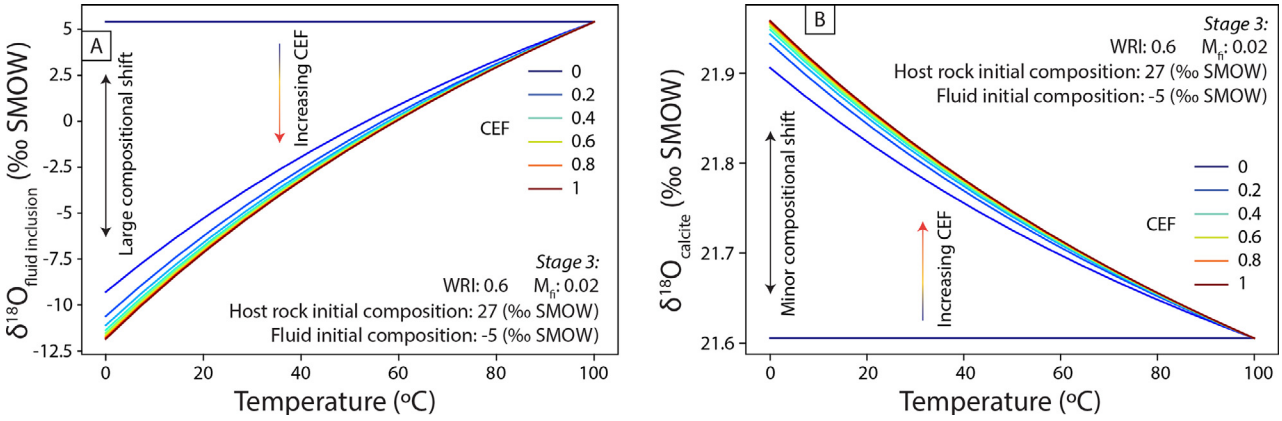

Fig. 7. Calculated $\delta^{18}O$ compositions of fluid inclusions (A) and calcite (B) formed at 100 °C and cooled down to 0 °C, resembling an uplift/exhumation scenario. The Calcite Exchange Fraction (CEF) varies between 0 to 1, while M_{fi}, the molar mass fraction of oxygen in the fluid inclusions, is kept at constant 0.02.

Facilitating the reset of the $T\alpha_{c\text{-}fi}$ and $T\Delta_{47}$ within the limits of CEF, the CEF exchange restriction causes an important decoupling between the paleothermometer values, even though their alteration results from the same dissolution-reprecipitation process. To illustrate this decoupling, if all calcite were available for recrystallization-induced isotope exchange during exhumation (i.e. CEF = 1), $T\alpha_{c\text{-}fi}$ and $T\Delta_{47}$ would record the same temperature during cooling and no decoupling between the paleothermometers would take place; both paleothermometers record T-values that correspond to the cooling temperatures (Fig. 8a; orange arrow cooling trajectory). In scenarios whereby an increasing portion of the calcite is excluded from isotopic exchange (i.e. CEF approaches zero), $T\Delta_{47}$ becomes increasingly insensitive to cooling, while $T\alpha_{c\text{-}fi}$ still responds strongly to the same amount of cooling (Fig. 8a; yellow arrow). The reason for this, is that the mass balance of oxygen between calcite and water is heavily skewed towards calcite ($M_{fi} = 0.02$); it dictates that the $\delta^{18}O_{fi}$ responds so strongly to slight temperature changes that $T\alpha_{c\text{-}fi}$ records near cooling temperatures, even if CEF approaches zero. If the porosity of the calcite vein, and thus the molar fraction of oxygen in water (M_{fi}) increases, the $\delta^{18}O_{fi}$ becomes less responsive to cooling and the $T\alpha_{c\text{-}fi}$ records temperatures higher than the actual ambient temperature (Fig. 8a–c; red arrows). Extreme scenarios of calcite porosity and its effect on the $T\alpha_{c\text{-}fi}$ versus $T\Delta_{47}$ array are visualised in Fig. 8b and c.

4.3. Solid-state diffusion

Isotope exchange processes also break and recreate C—O bonds by solid-state diffusion (Farver, 1994; Labotka et al., 2000), making the Δ_{47} composition of calcite minerals susceptible to overprinting at temperatures relevant to burial conditions (Passey and Henkes, 2012; Henkes et al., 2014; Stolper and Eiler, 2015; Lloyd et al., 2016; Brenner et al., 2018). However, as recrystallization reactions have a lower energetic barrier than solid-state processes (Bathurst, 1974; Baker et al., 1982), the dissolution-reprecipitation (i.e. recrystallization) reactions embody the primary mechanism by which the isotope compositions of carbonate minerals are altered at temperatures below 130 °C (Huntington et al., 2015), as are experienced by the calcite veins of this study. Nevertheless, it is important to note that solid-state diffusion potentially contributes to partial resetting of $T\Delta_{47}$, both inside and outside the exchangeable fraction and therefore the isotope exchange model should be regarded purely as a simplification.

The effect of solid-state diffusion on the Δ_{47} composition and corresponding temperature estimates was modelled using a Python script developed by Lloyd (2020), using regional T-t paths adopted from the same calciturbidite succession exposed in the nearby Kremenara anticline (Van Geet et al., 2002). The solid-state diffusion model uses calcite reordering parameters from Passey and Henkes (2012) and its re-fit by Stolper and Eiler (2015).

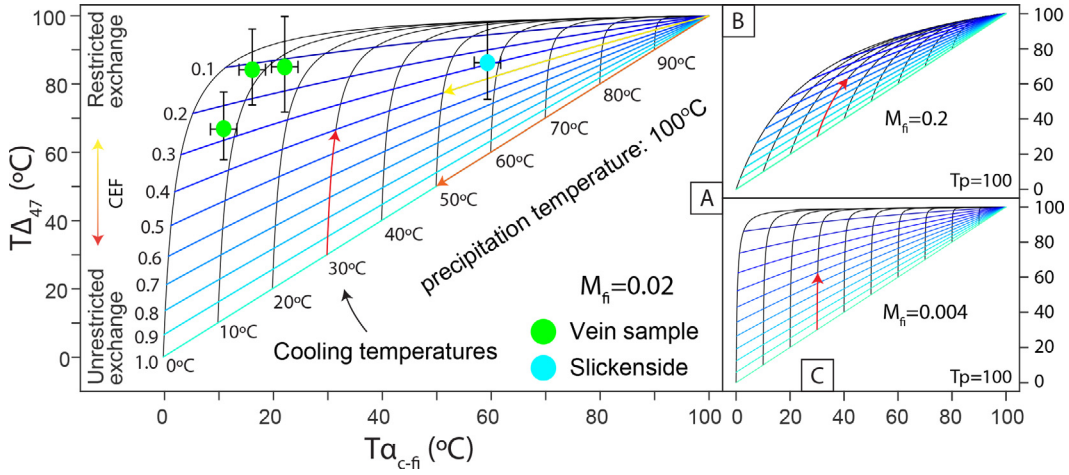

Fig. 8. (A) Simulations of the co-evolution of the $T\alpha_{c\text{-}fi}$ and Δ_{47} paleothermometers, for a vein sample cooling from 100 to 0 °C. The simulations show how the $T\alpha_{c\text{-}fi}$ and $T\Delta_{47}$ cooling trajectories respond to various Calcite Exchange Fractions (CEF), which range from 0 to 1, representing restricted and unrestricted exchange respectively. The orange arrow illustrates a cooling trajectory for a sample in which unrestricted exchange between calcite and fluid inclusions is possible (i.e. CEF = 1), during cooling from 100 °C to 50 °C. Measured $T\alpha_{c\text{-}fi}$ and $T\Delta_{47}$ from veins and a slickenside sample provide hypothetical constraints on the estimate of the CEF, provided the estimate of precipitation temperature is accurate for these samples. The red arrow highlights the difference in sensitivity of the $T\alpha_{c\text{-}fi}$ and Δ_{47} paleothermometers: a sample cooled from 100 °C to 30 °C at a CEF value of 0.4 will yield $T\alpha_{c\text{-}fi}$ values approximating 33 °C degrees, whilst $T\Delta_{47}$ values exceed 72 °C. It also illustrates that the Δ_{47} thermometer is relatively insensitive to changes in CEF at lower CEF values and becomes progressively more sensitive to changes in CEF at higher CEF values. Conversely, the $\alpha_{c\text{-}fi}$ thermometer is already very sensitive to slight increases from fully restricted to unrestricted isotope exchange and will readily record near cooling temperatures as isotope exchange becomes less restricted. However, the sensitivity of both paleothermometers to changes in CEF depends on size of the water reservoir in the calcite mineral: (B) and (C) show simulations of $T\alpha_{c\text{-}fi}$ and Δ_{47} co-variation with different oxygen mass distributions between calcite and fluid inclusions (M_{fi}). (For interpretation of the references to colour in this figure legend, the reader is referred to the web version of this article.)

Temperatures are calculated using the CDES25 temperature calibration (Schauble et al., 2006; Bonifacie et al., 2017). It is shown that, depending on the calcite reordering parameters, a maximum 3.8 °C can be accounted for by solid-state reordering at the timescales relevant to the Ionian Zone carbonates, provided that veins precipitate at or near surface temperatures (Appendix 3). Veins that precipitate at these burial temperatures remain virtually unaffected by solid-state diffusion.

4.4. Estimating CEF values and precipitation temperatures in natural samples: The External Albanides

The CEF value for any calcite sample formed at depth can thus be estimated by comparing its measured $T\alpha_{c\text{-}fi}$ and $T\Delta_{47}$ values to our modelled $T\alpha_{c\text{-}fi}$ and $T\Delta_{47}$ trajectories, provided that the initial precipitation temperature of the sample is known from independent temperature measurements (Fig. 9). *Vice versa*, if CEF values were precisely constrained or reliable estimates of CEF could be obtained from, for instance, petrographic observations, calcite precipitation temperatures may be estimated. From the previous exercise, it can be inferred that the $T\Delta_{47}$ value of an individual sample should be regarded as the minimum temperature at which calcite was formed, and that a discrepancy between corresponding $T\alpha_{c\text{-}fi}$ and $T\Delta_{47}$ values, is a CEF-dependent measure for how much temperature should be added to that minimum to come to a reliable estimate for the true precipitation temperature.

Fluid inclusion homogenisation temperatures of several vein samples from the External Albanides were previously reported to vary anywhere between 34 °C and 156 °C (Vilasi, 2009). Based on these temperatures, we have constructed $T\alpha_{c\text{-}fi}$ and $T\Delta_{47}$ cooling diagrams (Fig. 8). Constructing the cooling diagrams that correspond to several precipitation temperature intervals between 60 °C and 140 °C (Fig. 9) shows that the data are covered most fittingly by diagrams corresponding to precipitation temperatures of 80 °C and 100 °C, which is in concordance with independent estimates of local maximum burial temperatures for the Cretaceous-Paleogene calciturbidite interval (e.g. Roure et al., 2004). The vein samples record apparent isotope-exchange closure temperatures between 0 and 20 °C, significantly lower than the slickenside sample, which also records less discrepant $T\alpha_{c\text{-}fi}$ and $T\Delta_{47}$ values. This may be a result of a lower CEF value in these samples, if CEF is proportionate to time and the slickenside formed during a later stage in the tectonic development of the External Albanide fold and thrust belt. At the aforementioned precipitation temperatures, the CEF values of the vein samples range anywhere between 0 and 0.5, and exact precipitation temperatures, and therefore CEF values, remain poorly constrained. Our model shows how, at low CEF values, $T\Delta_{47}$ may be close to precipitation temperatures while fluid inclusions are overprinted.

4.5. Implications for the $\delta^{18}O$ composition of fluid inclusions

If we assume a standard CEF value for all vein samples, a hypothetical interpretation of the fluid-inclusion samples that were not analysed for clumped isotopes can be made. A CEF value allows for the calculation of isocompositional

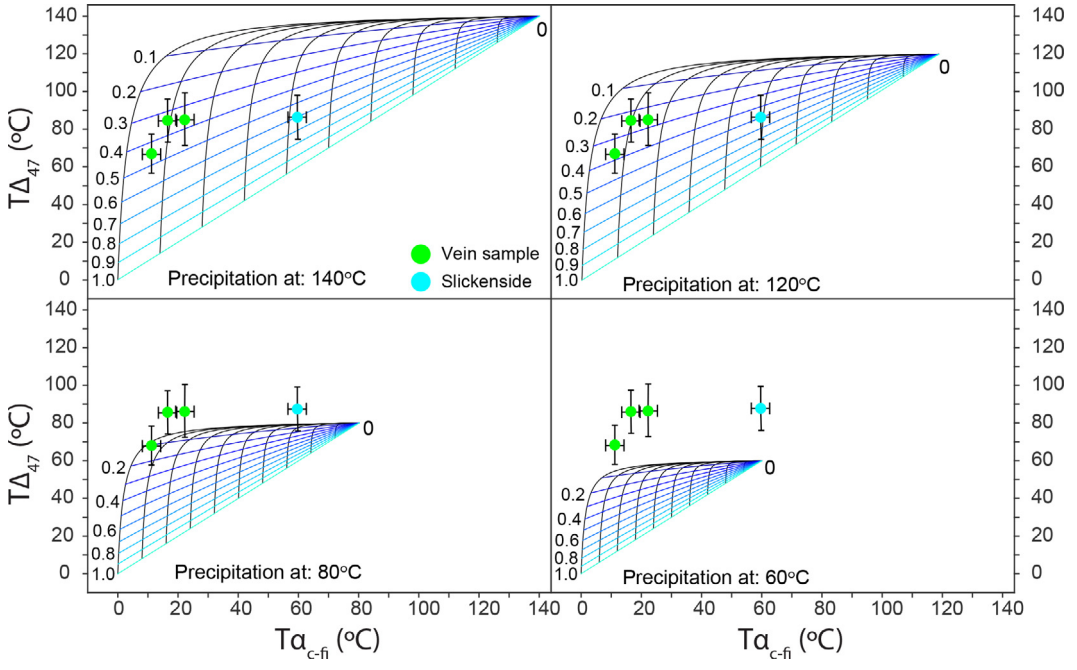

Fig. 9. Simulations of the co-evolution of the $T\alpha_{c\text{-}fi}$ and Δ_{47} paleothermometers at various CEFs, for calcite samples cooling from precipitation temperatures of 140 °C, 120 °C, 80 °C and 60 °C to 0 °C. The data derive from samples from the External Albanides (Appendix 1).

contours that correspond to $\delta^{18}O$ values of Stage 1 fluids as well as equilibrium closure temperatures, which is the temperature at which isotopic exchange between fluid inclusions and calcite no longer takes place (Fig. 10). The resulting array shows that, depending on this hypothetical equilibration closure temperature, the oxygen isotopic composition of fluid inclusions is offset approximately 1.5‰ per 10 °C using a maximum CEF value of 0.5. As the oxygen mass balance between calcite and fluid-inclusions is typically shifted towards calcite ($M_f = 0.02$), the isocompositional contours, and thus the recalculated parameters, appear to be fairly insensitive to changes in CEF. The isocompositional contours may provide estimates of the composition of subsurface fluids before burial (Fig. 1a). This particular exercise demonstrates how the compositional range of $\delta^{18}O_{fi}$ values may shift towards negative values as a result of the CEF-restricted oxygen isotope exchange during exhumation (Fig. 11).

The implication of this model on the fluid inclusion data of the External Albanides, is that reconstructed initial fluid $\delta^{18}O$ compositions plot between 1 and 15‰. Such high $\delta^{18}O$ values are commonly associated with fluids in magmatic systems and, therefore, appear somewhat unrealistic for the marine-meteoric fluid system of Albania. For this reason, it is interesting to determine to what extent the exchange model can account for the temperature offsets observed in the particular case of External Albanides. For example, the anomalously low $T\alpha_{c\text{-}fi}$ values that are recorded by some of the veins cannot solely be explained by oxygen isotope exchange. Possibly, these samples were affected by re-opening of the veins (Fig. 3) and the formation of secondary fluid inclusions with low, possibly purely meteoric $\delta^{18}O$ during the final stages of uplift. Alternatively, temperature offsets may be in place already during initial calcite precipitation due to out-of-equilibrium kinetic effects (Watkins et al., 2014; Daëron et al., 2019). Kinetic effects, however, depend largely on precipitation rates and CO_2 degassing, which are poorly constrained for these type of veins in general.

Despite the good fit of our data in the exchange model (Fig. 9), further research and modelling would be required to assess the actual effects of isotope exchange, secondary fluid inclusions and precipitation kinetics on temperature offsets in paleothermometers. Understanding the diagenetic stability of fluid inclusion water is of great importance for the accurate interpretation of fluid inclusion isotope records. More case studies are needed for different temperature domains and age ranges to test how widely applicable our model is to accurately predict calcite vein systems. Current information is scarce and lack systematics; other calcite vein systems of similar or older age do seem to produce realistic precipitation temperatures (de Graaf et al., 2017) or show at least partial exchange (Rye and O'Neil, 1968; de Graaf et al., 2020).

4.6. Implications of the CEF value

Based on a heating experiment (80 hours at 105 °C), Uemura et al. (2019) calculated that an increase of 0.7‰ $\delta^{18}O_{fi}$ was associated with a CEF value of 2% in speleothem calcite. Here, we suggest that higher CEF values in calcite veins may result from long-term (in order of millions of years) exposure to lowered temperatures, allowing recrystallization and associated oxygen isotope equilibration to

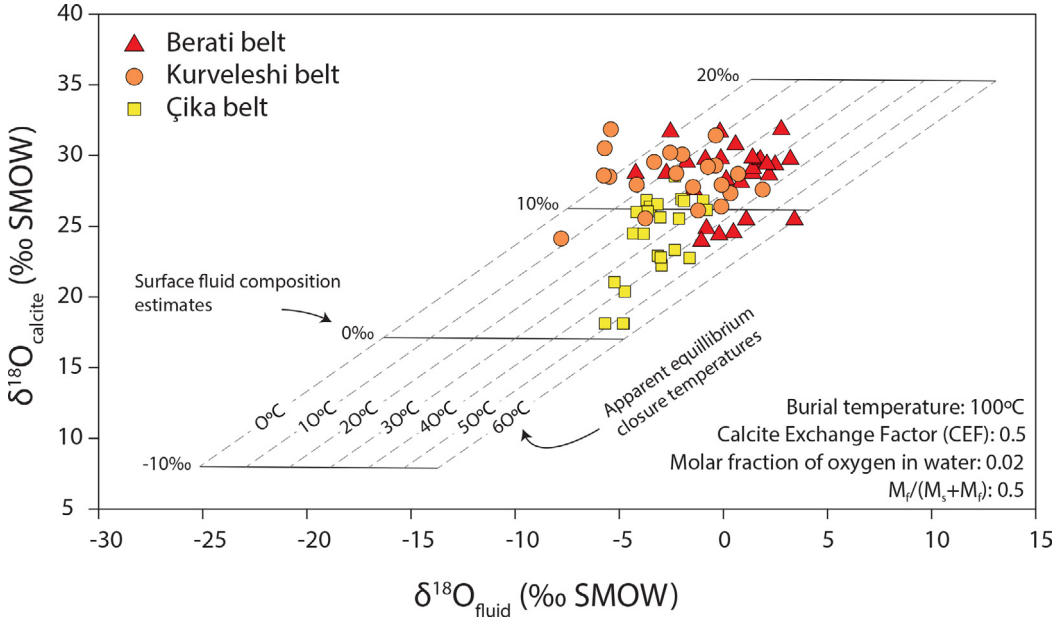

Fig. 10. Recalculated isocompositional contours of $\delta^{18}O$ composition of surficial water corresponding to Stage 1 of the batch fractionation model. Together with these compositions, a second set of isocompositional contours reflect $\delta^{18}O$ compositions that correspond to different equilibrium closure temperatures for oxygen isotope exchange. Fluid inclusion data suggest that the oxygen isotope composition of surface water from which calcite veins precipitated resembles the isotope composition of evaporated seawater at the time of infiltration. Oxygen isotope exchange appears to partially cease at temperatures <50 °C.

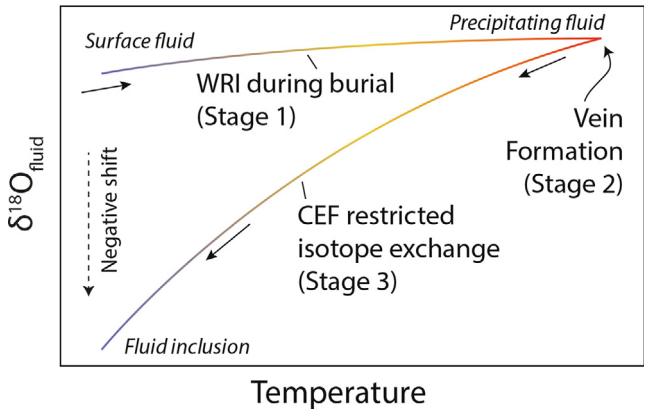

Fig. 11. Schematic representation of the fluid inclusion $\delta^{18}O$ composition during burial and uplift. The CEF-restricted isotope exchange results in lower $\delta^{18}O_{fi}$ values with respect to surface water.

have affected a larger part of the calcite vein. We speculate that the surface-area to fluid-abundance ratio (i.e. shape and size distribution) of fluid inclusions also could affect the CEF value. In our calcite vein samples, fluid inclusions generally have low perimeter-to-area ratios, as their shape is often elongated and follows crystal boundaries (Fig. 3). These crystal shapes are in contrast with fluid inclusions from, for instance, stalagmites, which are blocky-shaped, and thus have higher perimeter-to-area ratios (e.g. Van Breukelen et al., 2008; Krüger et al., 2011; Meckler et al., 2015). CEF may therefore vary depending on to mineralogical species of $CaCO_3$. Moreover, we have not considered that CEF may also be proportionate to time or temperature, which would significantly affect the sensitivity of the clumped isotope thermometer to diagenetic isotope exchange.

Nevertheless, this study demonstrates the importance of the CEF as it provides a likely mechanism by which $T\alpha_{c\text{-}fi}$ and $T\Delta_{47}$ of calcite veins decouple during cooling. Therefore, a better understanding of internal oxygen isotope exchange in carbonates is essential for interpreting the results that these commonly used paleothermometers yield. The combined application of $T\alpha_{c\text{-}fi}$ and $T\Delta_{47}$ may then become a useful indicator of sample alteration in calcium carbonates.

5. CONCLUSIONS

The fluid inclusion and clumped isotope thermometers are both vulnerable to re-equilibration during exhumation. At burial temperatures, fluid-mediated recrystallization is the dominant mode by which oxygen isotopes transfer between calcite and fluid inclusions. Here, we demonstrate how the $\alpha_{c\text{-}fi}$-and Δ_{47}-based paleothermometers in calcite may be altered by restricted isotope equilibration at temperatures below their initial precipitation temperatures and quantify how this affects the measured $T\alpha_{c\text{-}fi}$, $T\Delta_{47}$ and $\delta^{18}O_{fi}$ values of calcite samples.

Using mass-balance equilibration models, we simulated the co-evolution of $T\alpha_{c\text{-}fi}$ and $T\Delta_{47}$ for veins exhumed from various depths. We show that small degrees of oxygen isotope exchange between fluid inclusions and calcite induce significant changes in trapped fluid $\delta^{18}O$ values, as the distribution of oxygen between fluid inclusions and calcite is heavily shifted towards calcite. Our model shows that allowing a fraction of calcite to exchange oxygen isotopes with internal fluids affects the sensitivity of $T\alpha_{c\text{-}fi}$ and $T\Delta_{47}$ during exhumation: when limited isotope exchange is allowed, $T\alpha_{c\text{-}fi}$ becomes highly sensitive and will readily record cooling temperatures rather than record initial precipitation temperatures. $T\Delta_{47}$ is likewise affected by isotope exchange, but its values change to lesser degree than $T\alpha_{c\text{-}fi}$ so that during sample cooling, $T\Delta_{47}$ records higher temperatures.

In our case study, the extent of diagenetic alteration on $T\Delta_{47}$ remains poorly constrained; clumped isotope temperatures may be close to precipitation temperatures while fluid inclusions are overprinted and $T\alpha_{c\text{-}fi}$ records near cooling temperatures.

However, our model suggests that $T\Delta_{47}$ may change during sample cooling, if a relatively large amount of internal fluids is available or if a larger amount of oxygen in the calcite is available for isotope exchange with fluid inclusions, the Calcite Exchange Fraction (CEF). Our results emphasize that knowing the CEF value of a natural carbonate material determines its resilience to the effects of isotope exchange and the suitability for clumped isotope and calcite-fluid thermometry.

Declaration of Competing Interest

The authors declare that they have no known competing financial interests or personal relationships that could have appeared to influence the work reported in this paper.

ACKNOWLEDGEMENTS

We thank the School of Earth and Ocean Sciences at Cardiff University for hosting the first author during two research visits. We are thankful to Suzan Verdegaal for all technical support in the laboratory at Vrije Universiteit Amsterdam (The Netherlands). We acknowledge Bouke Lacet for manufacturing superb thin sections and are grateful to Sébastien Peter of Olympus Europa SE & Co. KG (Hamburg, Germany) for facilitating petrographic anal-

ysis of fluid inclusions by confocal laser scanning microscopy. Furthermore, we have very much appreciated the thoughtful and constructive reviews of the editor and four anonymous reviewers, because of whom the manuscript has improved significantly. This study was partially sponsored by CPG-KFUPM (Dhahran, KSA) start-up funds to JR. MZ acknowledges funding through the NWO VIDI project 016.161.365, which is financed by the Netherlands Organization for Scientific Research (NWO). This paper is part of the first authors PhD thesis.

APPENDIX A. SUPPLEMENTARY MATERIAL

Supplementary data to this article can be found online at https://doi.org/10.1016/j.gca.2020.12.008.

REFERENCES

Affolter S., Fleitmann D. and Leuenberger M. (2014) New online method for water isotope analysis of speleothem fluid inclusions using laser absorption spectroscopy (WS-CRDS). *Clim. Past* **10**, 1291–1304.

Arienzo M. M., Swart P. K. and Vonhof H. B. (2013) Measurement of $\delta^{18}O$ and $\delta^{2}H$ values of fluid inclusion water in speleothems using cavity ring-down spectroscopy compared with isotope ratio mass spectrometry. *Rapid Commun. Mass Spectrom.* **27**, 2616–2624.

Baker P. A., Gieskes J. M. and Elderfield H. (1982) Diagenesis of carbonates in deep-sea sediments – Evidence from Sr/Ca ratios and interstitial dissolved Sr^{2+} data. *J. Sediment. Petrol.* **52**, 71–82.

Bathurst R. G. C. (1974) Marine diagenesis of shallow water calcium carbonate sediments. *Annu. Rev. Earth Planet. Sci.* **2**, 257–274.

Beinlich A., Plümper O., Boter E., Müller I. A., Kourim F., Ziegler M., Harigane Y., Lafay R. and Kelemen P. B. (2020) Ultramafic rock carbonation: Constraints from Listvenite Core BT1B, Oman Drilling Project. *J. Geophys. Res. Solid Earth* **125**.

Bergman S. C., Huntington K. W. and Crider J. G. (2013) Tracing paleofluid sources using clumped isotope thermometry of diagenetic cements along the Moab Fault, Utah. *Am. J. Sci.* **313**, 490–515.

Bernasconi S. M., Müller I. A., Bergmann K. D., Breitenbach S. F. M., Fernandez A., Hodell D. A., Jaggi M., Meckler A. N., Millan I. and Ziegler M. (2018) Reducing uncertainties in carbonate clumped isotope analysis through consistent carbonate-based standardization. *Geochemi. Geophys. Geosyst.* **19**, 2895–2914.

Bonifacie M., Calmels D., Eiler J. M., Horita J., Chaduteau C., Vasconcelos C., Agrinier P., Katz A., Passey B. H., Ferry J. M. and Bourrand J. J. (2017) Calibration of the dolomite clumped isotope thermometer from 25 to 350°C, and implications for a universal calibration for all (Ca, Mg, Fe)CO_3 carbonates. *Geochim. Cosmochim. Acta* **200**, 255–279.

Brand W. A., Assonov S. S. and Coplen T. B. (2010) Correction for the ^{17}O interference in δ(13C) measurements when analyzing CO_2 with stable isotope mass spectrometry (IUPAC Technical Report). *Pure Appl. Chem.* **82**, 1719–1733.

Brenner D. C., Passey B. H. and Stolper D. A. (2018) Influence of water on clumped-isotope bond reordering kinetics in calcite. *Geochim. Cosmochim. Acta* **224**, 42–63.

Van Breukelen M. R., Vonhof H. B., Hellstrom J. C., Wester W. C. G. and Kroon D. (2008) Fossil dripwater in stalagmites reveals Holocene temperature and rainfall variation in Amazonia. *Earth Planet. Sci. Lett.* **275**, 54–60.

Budd D. A., Frost E. L., Huntington K. W. and Allwardt P. F. (2013) Syndepositional deformation features in high-relief carbonate platforms: long-lived conduits for diagenetic fluids. *J. Sediment. Res.* **82**, 12–36.

Burgener L. K., Huntington K. W., Sletten R., Watkins J. M., Quade J. and Hallet B. (2018) Clumped isotope constraints on equilibrium carbonate formation and kinetic isotope effects in freezing soils. *Geochim. Cosmochim. Acta* **235**, 402–430.

Coplen T. B. (2007) Calibration of the calcite–water oxygen-isotope geothermometer at Devils Hole, Nevada, a natural laboratory. *Geochim. Cosmochim. Acta* **71**, 3948–3957.

Daëron M., Blamart D., Peral M. and Affek H. P. (2016) Absolute isotopic abundance ratios and the accuracy of D47 measurements. *Chem. Geol.* **441**, 83–96.

Daëron M., Drysdale R. N., Peral M., Huyghe D., Blamart D., Coplen T. B., Lartaud F. and Zanchetta G. (2019) Most Earth-surface calcites precipitate out of isotopic equilibrium. *Nat. Commun.* **10**.

Dennis K. J., Cochran J. K., Landman N. H. and Schrag D. P. (2013) The climate of the Late Cretaceous: New insights from the application of the carbonate clumped isotope thermometer to Western Interior Seaway macrofossil. *Earth Planet. Sci. Lett.* **362**, 51–65.

Dennis P., Rowe P. and Atkinson T. (2001) The recovery and isotopic measurement of water from fluid inclusions in speleothems. *Geochim. Cosmochim. Acta* **65**, 871–884.

Dublyansky Y. V. and Spötl C. (2009) Hydrogen and oxygen isotopes of water from inclusions in minerals: design of a new crushing system and on-line continuous-flow isotope ratio mass spectrometric analysis. *Rapid Commun. Mass Spectrom.* **23**, 2605–2613.

Elias Bahnan A., Carpentier C., Pironon J., Ford M., Ducoux M., Barré G., Mangenot X. and Gaucher E. C. (2020) Impact of geodynamics on fluid circulation and diagenesis of carbonate reservoirs in a foreland basin: Example of the Upper Lacq reservoir (Aquitaine basin, SW France). *Mar. Pet. Geol.* **111**, 676–694.

Epstein S. and Mayeda T. (1953) Variation of O18 content of waters from natural sources. *Geochim. Cosmochim. Acta* **4**, 213–224.

Farver J. R. (1994) Oxygen self-diffusion in calcite: Dependence on temperature and water fugacity. *Earth Planet. Sci. Lett.* **121**, 575–587.

Finnegan S., Bergmann K., Eiler J. M., Jones D. S., Fike D. A., Eisenman I., Hughes N. C., Tripati A. K. and Fischer W. W. (2011) The magnitude and duration of late Ordovician-early Silurian glaciation. *Science (80-.)* **331**, 903–906.

Fosu B. R., Ghosh P. and Viladkar S. G. (2020) Clumped isotope geochemistry of carbonatites in the north-western Deccan igneous province: Aspects of evolution, post-depositional alteration and mineralisation. *Geochim. Cosmochim. Acta* **274**, 118–135.

Van Geet M., Swennen R., Durmishi C., Roure F. and Muchez P. H. (2002) Paragenesis of Cretaceous to Eocene carbonate reservoirs in the Ionian fold and thrust belt (Albania): Relation between tectonism and fluid flow. *Sedimentology* **49**, 697–718.

Ghosh P., Adkins J., Affek H., Balta B., Guo W., Schauble E. A., Schrag D. and Eiler J. M. (2006) 13C–18O bonds in carbonate minerals: A new kind of paleothermometer. *Geochim. Cosmochim. Acta* **70**, 1439–1456.

Le Goff J., Cerepi A., Swennen R., Loisy C., Caron M., Muska K. and El Desouky H. (2015) Contribution to the understanding of the Ionian Basin sedimentary evolution along the eastern edge of Apulia during the Late Cretaceous in Albania. *Sediment. Geol.* **317**, 87–101.

Le Goff J., Reijmer J. J. G., Cerepi A., Loisy C., Swennen R., Heba G., Cavailhes T. and De Graaf S. (2019) The dismantling of the Apulian carbonate platform during the late Campanian – early Maastrichtian in Albania. *Cretac. Res.* **96**, 83–106.

de Graaf S., Lüders V., Banks D. A., Sośnicka M., Reijmer J. J. G., Kaden H. and Vonhof H. B. (2020) Fluid evolution and ore deposition in the Harz Mountains revisited: isotope and crush-leach analyses of fluid inclusions. *Miner. Depos.* **55**, 47–62.

de Graaf S., Nooitgedacht C. W., Le Goff J., van der Lubbe J. (H). J. L., Vonhof H. B. and Reijmer J. J. G. (2019) Fluid flow evolution in the Albanide fold-and-thrust belt: Insights from δ2H and δ18O isotope ratios of fluid inclusions. *Am. Assoc. Pet. Geol. Bull.*.

de Graaf S., Reijmer J. J. G., Bertotti G. V., Bezerra F. H. R., Cazarin C. L., Bisdom K. and Vonhof H. B. (2017) Fracturing and calcite cementation controlling fluid flow in the shallow-water carbonates of the Jandaíra Formation, Brazil. *Mar. Pet. Geol.* **80**, 382–393.

Graham Wall B. R., Girbacea R., Mesonjesi A. and Aydin A. (2006) Evolution of fracture and fault-controlled fluid pathways in carbonates of the Albanides fold-thrust belt. *Am. Assoc. Pet. Geol. Bull.* **90**, 1227–1249.

Henkes G. A., Passey B. H., Grossman E. L., Shenton B. J., Pérez-Huerta A. and Yancey T. E. (2014) Temperature limits for preservation of primary calcite clumped isotope paleotemperatures. *Geochim. Cosmochim. Acta* **139**, 362–382.

Honlet R., Gasparrini M., Muchez P., Swennen R. and John C. M. (2018) A new approach to geobarometry by combining fluid inclusion and clumped isotope thermometry in hydrothermal carbonates. *Terra Nov.* **30**, 199–206.

Huntington K. W., Budd D. A., Wernicke B. P. and Eiler J. M. (2011) Use of clumped-isotope thermometry to constrain the crystallization temperature of diagenetic calcite. *J. Sediment. Res.* **81**, 656–669.

Huntington K. W. and Lechler A. R. (2015) Carbonate clumped isotope thermometry in continental tectonics. *Tectonophysics* **647–648**, 1–20.

Huntington K. W., Saylor J., Quade J. and Hudson A. M. (2015) High late Miocene-Pliocene elevation of the Zhada Basin, southwestern Tibetan Plateau, from carbonate clumped isotope thermometry. *Geol. Soc. Am. Bull.* **127**, 181–199.

Kele S., Breitenbach S. F. M., Capezzuoli E., Meckler A. N., Ziegler M., Millan I. M., Kluge T., Deák J., Hanselmann K., John C. M., Yan H., Liu Z. and Bernasconi S. M. (2015) Temperature dependence of oxygen- and clumped isotope fractionation in carbonates: A study of travertines and tufas in the 6–95 °C temperature range. *Geochim. Cosmochim. Acta* **168**, 172–192.

Kelson J. R., Huntington K. W., Breecker D. O., Burgener L. K., Gallagher T. M., Hoke G. D. and Petersen S. V. (2020) A proxy for all seasons? A synthesis of clumped isotope data from Holocene soil carbonates. *Quat. Sci. Rev.* **234**, 106259.

Kim S.-T. and O'Neil J. R. (1997) Equilibrium and nonequilibrium oxygen isotope effects in synthetic carbonates. *Geochim. Cosmochim. Acta* **61**, 3461–3475.

Knauth L. P. and Kennedy M. J. (2009) The late Precambrian greening of the Earth. *Nature* **460**, 728–732.

Kocken I. J., Müller I. A. and Ziegler M. (2019) Optimizing the use of carbonate standards to minimize uncertainties in clumped isotope data. *Geochem. Geophys. Geosyst.* **20**, 5565–5577.

Krüger Y., Marti D., Staub R. H., Fleitmann D. and Frenz M. (2011) Liquid-vapour homogenisation of fluid inclusions in stalagmites: Evaluation of a new thermometer for palaeoclimate research. *Chem. Geol.* **289**, 39–47.

Labotka T. C., Cole D. R. and Riciputi L. R. (2000) Diffusion of C and O in calcite at 100 MPa. *Am. Mineral.* **85**, 488–494.

Lacombe O., Malandain J., Vilasi N., Amrouch K. and Roure F. (2009) From paleostresses to paleoburial in fold–thrust belts: Preliminary results from calcite twin analysis in the Outer Albanides. *Tectonophysics* **475**, 128–141.

Lacroix B. and Niemi N. A. (2019) Investigating the effect of burial histories on the clumped isotope thermometer: An example from the Green River and Washakie Basins, Wyoming. *Geochim. Cosmochim. Acta* **247**, 40–58.

Lacroix B., Travé A., Buatier M., Labaume P., Vennemann T. and Dubois M. (2014) Syntectonic fluid-flow along thrust faults: Example of the South-Pyrenean fold-and-thrust belt. *Mar. Pet. Geol.* **49**, 84–98.

Lloyd, M.K., 2020. ClumpyCool.

Lloyd M. K., Eiler M. K. and Nabelek J. M. (2016) Clumped isotope thermometry of calcite and dolomite in a contact metamorphic environment. *Geochim. Cosmochim. Acta*.

Luetkemeyer P. B., Kirschner D. L., Huntington K. W., Chester J. S., Chestercchester F. M. and Evans J. P. (2016) Constraints on paleofluid sources using the clumped-isotope thermometry of carbonate veins from the SAFOD (San Andreas Fault Observatory at Depth) borehole. *Tectonophysics* **690**, 174–189.

Macdonald J. M., John C. M. and Girard J. P. (2018) Testing clumped isotopes as a reservoir characterization tool: A comparison with fluid inclusions in a dolomitized sedimentary carbonate reservoir buried to 2–4 km. *Geol. Soc. Spec. Publ.* **468**, 189–202.

Mangenot X., Bonifacie M., Gasparrini M., Götz A., Chaduteau C., Ader M. and Rouchon V. (2017) Coupling Δ47 and fluid inclusion thermometry on carbonate cements to precisely reconstruct the temperature, salinity and δ18O of paleo-groundwater in sedimentary basins. *Chem. Geol.* **472**, 44–57.

McCrea J. M. (1950) On the isotopic chemistry of carbonates and a paleotemperature scale. *J. Chem. Phys.* **18**, 849–857.

Meckler A. N., Affolter S., Dublyansky Y. V., Krüger Y., Vogel N., Bernasconi S. M., Frenz M., Kipfer R., Leuenberger M., Spötl C., Carolin S., Cobb K. M., Moerman J., Adkins J. F. and Fleitmann D. (2015) Glacial-interglacial temperature change in the tropical West Pacific: A comparison of stalagmite-based paleo-thermometers. *Quat. Sci. Rev.* **127**, 90–116.

Meckler A. N., Ziegler M., Millán M. I., Breitenbach S. F. M. and Bernasconi S. M. (2014) Long-term performance of the Kiel carbonate device with a new correction scheme for clumped isotope measurements. *Rapid Commun. Mass Spectrom.* **28**, 1705–1715.

Meço S., Aliaj S. and Turku I. (2000) *Geology of Albania*. Gebrüder Borntraeger.

Methner K., Mulch A., Fiebig J., Wacker U., Gerdes A., Graham S. A. and Chamberlain C. P. (2016) Rapid Middle Eocene temperature change in western North America. *Earth Planet. Sci. Lett.* **450**, 132–139.

Müller I. A., Fernandez A., Radke J., van Dijk J., Bowen D., Schwieters J. and Bernasconi S. M. (2017a) Carbonate clumped isotope analyses with the long-integration dual-inlet (LIDI) workflow: scratching at the lower sample weight boundaries. *Rapid Commun. Mass Spectrom.* **31**, 1057–1066.

Müller P., Staudigel P. T., Murray S. T., Vernet R., Barusseau J. P., Westphal H. and Swart P. K. (2017b) Prehistoric cooking versus accurate palaeotemperature records in shell midden constituents. *Sci. Rep.* **7**, 1–11.

Naylor H. N., Defliese W. F., Grossman E. L. and Maupin C. R. (2019) Investigation of the thermal history of the Delaware Basin (West Texas, USA) using carbonate clumped isotope thermometry. *Basin Res.*, bre.12419.

Nieuwland D. A., Oudmayer B. C. and Valbona U. (2001) The tectonic development of Albania: Explanation and prediction of structural styles. *Mar. Pet. Geol.* **18**, 161–177.

Pagel M., Bonifacie M., Schneider D. A., Gautheron C., Brigaud B., Calmels D., Cros A., Saint-Bezar B., Landrein P., Sutcliffe C., Davis D. and Chaduteau C. (2018) Improving paleohydrological and diagenetic reconstructions in calcite veins and breccia of a sedimentary basin by combining Δ_{47} temperature, $\delta^{18}O_{water}$ and U-Pb age. *Chem. Geol.* **481**, 1–17.

Passey B. H. and Henkes G. A. (2012) Carbonate clumped isotope bond reordering and geospeedometry. *Earth Planet. Sci. Lett.* **351–352**, 223–236.

Price G. D. and Passey B. H. (2013) Dynamic polar climates in a greenhouse world: Evidence from clumped isotope thermometry of early cretaceous belemnites. *Geology* **41**, 923–926.

Roure F., Nazaj S., Mushka K., Fili I., Cadet J.-P. and Bonneau M. (2004) Kinematic evolution and petroleum systems-an appraisal of the outer Albanides. *AAPG Mem.* **82**, 474–493.

Rye R. O. and O'Neil J. R. (1968) The O18 content of water in primary fluid inclusions from Providencia, north-central Mexico. *Econ. Geol.* **63**, 232–238.

Sample J. C., Torres M. E., Fisher A., Hong W.-L., Destrigneville C., Defliese W. F. and Tripati A. E. (2017) Geochemical constraints on the temperature and timing of carbonate formation and lithification in the Nankai Trough, NanTroSEIZE transect. *Geochim. Cosmochim. Acta* **198**, 92–114.

Schauble E. A., Ghosh P. and Eiler J. M. (2006) Preferential formation of 13C–18O bonds in carbonate minerals, estimated using first-principles lattice dynamics. *Geochim. Cosmochim. Acta* **70**, 2510–2529.

Snell K. E., Thrasher B. L., Eiler J. M., Koch P. L., Sloan L. C. and Tabor N. J. (2013) Hot summers in the Bighorn Basin during the early Paleogene. *Geology* **41**, 55–58.

Staudigel P. T., Murray S., Dunham D. P., Frank T. D., Fielding C. R. and Swart P. K. (2018) Cryogenic brines as diagenetic fluids: Reconstructing the diagenetic history of the Victoria Land Basin using clumped isotopes. *Geochim. Cosmochim. Acta* **224**, 154–170.

Staudigel P. T. and Swart P. K. (2019) A diagenetic origin for isotopic variability of sediments deposited on the margin of Great Bahama Bank, insights from clumped isotopes. *Geochim. Cosmochim. Acta* **258**, 97–119.

Staudigel P. T., Swart P. K., Pourmand A., Laguer-Díaz C. A. and Pestle W. J. (2019) Boiled or roasted? Bivalve cooking methods of early Puerto Ricans elucidated using clumped isotopes. *Sci. Adv.* **5**, 5447–5474.

Stolper D. A. and Eiler J. M. (2015) The kinetics of solid-state isotope-exchange reactions for clumped isotopes: A study of inorganic calcites and apatites from natural and experimental samples. *Am. J. Sci.* **315**, 363–411.

Stolper D. A., Eiler J. M. and Higgins J. A. (2018) Modeling the effects of diagenesis on carbonate clumped-isotope values in deep- and shallow-water settings. *Geochim. Cosmochim. Acta* **227**, 264–291.

Sundell K. E., Saylor J. E., Lapen T. J. and Horton B. K. (2019) Implications of variable late Cenozoic surface uplift across the Peruvian central Andes. *Sci. Rep.*, 9.

Tremaine D. M., Froelich P. N. and Wang Y. (2011) Speleothem calcite farmed in situ: Modern calibration of δ18O and δ13C paleoclimate proxies in a continuously-monitored natural cave system. *Geochim. Cosmochim. Acta* **75**, 4929–4950.

Uemura R., Kina Y. and Omine K. (2019) Experimental evaluation of oxygen isotopic exchange between inclusion water and host calcite in speleothems. *Clim. Past Discuss.* **3**, 1–18.

Uemura R., Nakamoto M., Asami R., Mishima S., Gibo M., Masaka K., Jin-Ping C., Wu C.-C., Chang Y.-W. and Shen C.-C. (2016) Precise oxygen and hydrogen isotope determination in nanoliter quantities of speleothem inclusion water by cavity ring-down spectroscopic techniques. *Geochim. Cosmochim. Acta* **172**, 159–176.

Velaj T. (2015) New ideas on the tectonic of the Kurveleshi anticlinal belt in Albania, and the perspective for exploration in its subthrust. *Petroleum* **1**, 269–288.

Velaj T., Davison I., Serjani A. and Alsop I. (1999) Thrust tectonics and the role of evaporites in the Ionian Zone of the Albanides. *Am. Assoc. Pet. Geol. Bull.* **83**, 1408–1425.

Vilasi N. (2009) *Etude d'analogues de réservoirs dans les chaînes plissées et leurs avant- pays: Sédimentologie, diagenèse, déformation et fracturation des systèmes carbonatés crétacés supérieurs - éocènes du Bassin Ionien (Albanie méridionale)*. Mines ParisTech.

Vilasi N., Swennen R. and Roure F. (2006) Diagenesis and fracturing of Paleocene-Eocene carbonate turbidite systems in the Ionian Basin: The example of the Kelçyra area (Albania). *J. Geochem. Explor.* **89**, 409–413.

Vonhof H. B., van Breukelen M. R., Postma O., Rowe P. J., Atkinson T. C. and Kroon D. (2006) A continuous-flow crushing device for on-line δ2H analysis of fluid inclusion water in speleothems. *Rapid Commun. Mass Spectrom.* **20**, 2553–2558.

Watkins J. M. and Hunt J. D. (2015) A process-based model for non-equilibrium clumped isotope effects in carbonates. *Earth Planet. Sci. Lett.* **432**, 152–165.

Watkins J. M., Hunt J. D., Ryerson F. J. and Depaolo D. J. (2014) The influence of temperature, pH, and growth rate on the δ18O composition of inorganically precipitated calcite. *Earth Planet. Sci. Lett.* **404**, 332–343.

Wierzbowski H., Bajnai D., Wacker U., Rogov M. A., Fiebig J. and Tesakova E. M. (2018) Clumped isotope record of salinity variations in the Subboreal Province at the Middle-Late Jurassic transition. *Glob. Planet. Change* **167**, 172–189.

Winkelstern I. Z. and Lohmann K. C. (2016) Shallow burial alteration of dolomite and limestone clumped isotope geochemistry. *Geology* **44**, 467–470.

Associate editor: Cedric Michael John